Environmental Science and Pollution Research (2022) 29:77188–77198
https://doi.org/10.1007/s11356-022-21193-y

RESEARCH ARTICLE

Effect of pH, ionic strength, and temperature on the adsorption behavior of Acid Blue 113 onto mesoporous carbon

Rosembergue Gabriel Lima Gonçalves[1] · Paloma Aparecida Lopes[1] · Daniel José Pochapski[2] · Luiz Carlos Alves de Oliveira[3] · Frederico Garcia Pinto[4] · Jonas Leal Neto[1] · Jairo Tronto[4]

Received: 17 January 2022 / Accepted: 26 May 2022 / Published online: 8 June 2022

Abstract

Mesoporous carbon (MC) derived from cassava starch was used to remove Acid Blue 113 azo dye from aqueous solutions. The influence of temperature, pH, ionic strength, and the adsorbent dose was investigated in a set of batch experiments. Experimental data showed that Acid Blue 113 adsorption was higher in the acid pH range than in the alkaline one, that dye adsorption increases when the ionic strength and temperature increase, and that adsorption results presented a good correlation with the Langmuir isotherm model. The adsorption capacity of MC was 295 mg g^{-1}, at pH = 7.0 and 298 K, respectively. Zeta potential (ζ) showed the compression of the diffuse double layer of adsorbent with an increase in temperature and ionic strength, promoting the decrease of electrostatic repulsion between the negatively charged surface of the carbon particles and the anionic dye. Thermodynamic results demonstrate that the adsorption process was spontaneous and endothermic. Moreover, for the first time, this work has demonstrated that the pH, temperature, and ionic strength of the aqueous medium are also able to change the surface charge of carbon-based adsorbents and surely influence the adsorption capacity. Finally, the regeneration of the adsorbent by the photo-Fenton reaction regenerated the adsorption capacity of the adsorbent without generating secondary pollution to the environment.

Keywords Mesoporous carbon · Acid Blue 113 · Sacrifice template · Textile dyes · Reusable adsorbent · Electrostatic interactions

Introduction

The increase in water pollution by fertilizers, pesticides, and industrial chemicals, becomes potable water grows an increasingly scarce resource (Hamza et al. 2018; Singh et al. 2020). Though the earth is covered with plenty of water, the amount of drinkable water is finite. Therefore, wastewater treatments and water reuse are the best options to minimize environmental damage and stress on groundwater resources (Luo et al. 2014; Hao et al. 2019). Among various organic contaminants discarded in surface waters, the dyes, surfactants, and phenolic compounds are the ones that stand out the most due to the high concentrations and massive use in industrial and commercial processes worldwide (Taffarel and Rubio 2010; Luo et al. 2014; dos Santos et al. 2018; Zhang et al. 2018; Liu et al. 2020). Besides, they are toxic to aquatic fauna and flora and may contribute to important water quality parameter changes (Borrely et al. 2018; Xu et al. 2020).

Responsible Editor: Tito Roberto Cadaval Jr

✉ Rosembergue Gabriel Lima Gonçalves
rosemberguegabriel@hotmail.com

✉ Jairo Tronto
jairotronto@ufv.br

[1] Department of Chemistry, Federal University of Lavras, C.P. 3037, Lavras, MG CEP 37.200-000, Brazil

[2] Institute of Chemistry, São Paulo State University (UNESP), Av. Professor Francisco Degni, 55, Araraquara, SP CEP 14.800-900, Brazil

[3] Chemistry Department, ICEx, Federal University of Minas Gerais, Av. Antônio Carlos, 6627, Belo Horizonte, MG CEP 31.270-901, Brazil

[4] Institute of Exact Sciences and Technology, Federal University of Viçosa, Rio Paranaíba Campus, Rodovia MG 230, km 7, Rio Paranaíba, MG CEP 38.810-000, Brazil

In wastewater treatment, recalcitrant compounds removal by adsorption stands out as the main separation technique due to features such as lower energy consumption, simplicity of use, and adaptability (Fahel et al. 2016). Among the most used adsorbents in the literature, carbonaceous materials such as activated carbon (Tian et al. 2018), mesoporous carbon (MC) (Hu et al. 2019; Azam et al. 2020), graphene (Rajumon et al. 2019; Cao et al. 2019), and carbon nanotubes (Xu et al. 2018) stand out for their low toxicity, high porosity, and good performance on organic and inorganic contaminants removal from water (Yang et al. 2015; Xu et al. 2018). As for the application of these materials, many studies have shown that the presence of large pores improves the removal of bulky organic molecules from aqueous solution, as the exclusive presence of micropores prevents the entry of large molecules such as azo dyes and proteins into the pores (Gupta et al. 2011; Qiang et al. 2016; Tokudome et al. 2016). Thus, predominantly microporous adsorbents such as activated carbon have a lower adsorption capacity for large molecules than mesoporous carbon materials (Ip et al. 2009; Gupta et al. 2011; Parker et al. 2012; Qiang et al. 2016).

Despite their high toxicity, azo dyes are among the bulky organic molecules most applied in adsorption science. Due to their properties of good adhesion and high stability, these molecules stand out for their wide use in the textile industry (mainly in wool, polyamide, and plastic productions) (Gupta et al. 2011; Samarghandi et al. 2020). These molecules are often in an irresponsibly manner thrown into water effluents causing problems to aquatic biota and human health because they are highly toxic and potentially carcinogenic (Vikrant et al. 2018; Lellis et al. 2019). To prevent environmental contamination, several studies have been performed using adsorbents such as clays, activated carbon, and biochar to remove azo dyes such as AB113 from wastewater of textile industries (Yagub et al. 2014). However, to justify the adsorption capacity, these studies do not evaluate what happens to the surface charge of the adsorbent when the aqueous solution medium condition such as ionic strength and temperature are changed. Therefore, the performance of this study is still required to evaluate the real contributions of the superficial charge of adsorbents in the adsorption process.

Despite the satisfactory results of removal of the organic compounds such as dyes, surfactants, and phenolic compounds (Chiang et al. 2020), the regeneration/reuse of carbonaceous materials remains a great challenge because regeneration methods such as solvent extraction, thermal regeneration, basic extraction, and chemical oxidation (Chen et al. 2011; Vecitis et al. 2011; Pinto et al. 2018; Azha et al. 2019; Marrakchi et al. 2020; Du et al. 2020) require a lot of time, high energy consumption, and large quantities of chemical reagents.

Based on the above findings, the objective of this work was to study the feasibility of using MC derived from cassava starch (*Manihot esculenta* Crantz) as an adsorbent for Acid Blue 113 from aqueous solutions. The influence of solution pH, ionic strength, and temperature on AB113 adsorption were evaluated and correlated with ζ-potential of MC. This work also reports the use of advanced oxidation processes (AOPs) as an alternative method for the MC regeneration/reuse after adsorption of azo dye Acid Blue 113 (AB113).

Experimental

Materials

Laponite (sodium hectorite) was obtained from Laporte Industry; AB113 was obtained from BASF Industry, and the cassava starch was obtained from Amafil Company.

MC preparation was based on an adaptation of the methodology developed previously (Pinto et al. 2016). Briefly, in this synthesis, MC was prepared by mixing the Laponite clay exfoliated with starch gel. Then the resulting material was dried at 338 K and calcined at 1073 K under N_2 atmosphere for 2 h. Lastly, the calcined material was treated with 0.25 L of HF solution (20% (v/v)) and 0.25 L of HCl solution (6 mol L^{-1}) for 24 h for the dissolution of the clay. After the clay removal, the powder was washed and dried at 373 K.

Characterization methods

The material produced was characterized by X-ray diffraction (XRD) using a Shimadzu XRD-6000 diffractometer with graphite crystal as a monochromator to select Cu-Kα_1 radiation ($\lambda = 1.5406$ Å), with a scanning rate of 0.02° s^{-1}. The morphology of the produced materials was analyzed by scanning electron microscopy (SEM), using a Quanta 3D FEG microscope. The samples were coated with gold before measurements, using a Sputter BALTEC, MED 0.20, and fixed to the sample holder by conductive, double-sided tape. The N_2 adsorption/desorption isotherms at 77 K were obtained in an Autosorb Quantachrome. Energy-dispersive X-ray spectroscopy (EDS) was carried out using a Jeol Model JXA-8900RL instrument. Raman spectra were recorded by FT-Raman Bruker Vertex 70.

Zeta potential analysis

The ZetaSizer analyzer (ZetaSizer Nano SZ Malvern Instruments Ltd., UK, attached to an MPT-2 Autotitrator) was used to determine the electrophoretic mobility (μ) of MC particles. To determine the influence of pH value, ionic strength, and temperature on zeta potential values, 0.005 g of MC was dispersed in NaCl solutions (0.001 mol L^{-1} and 0.1 mol L^{-1}). The measurements were carried out at different

temperatures (273–308 K), and the pH value was adjusted using HCl (0.20 mol L^{-1}) or NaOH (0.20 mol L^{-1}) solutions.

To calculate the zeta potential (ζ) values of MC particles, the Helmholtz-Smoluchowski equation was used. This equation is the most widely used relationship for relating the electrophoretic mobility of a colloidal particle its zeta potential (Agnihotri et al. 2009),

$$\mu = \frac{\varepsilon_r \varepsilon_0}{\eta} \zeta \tag{1}$$

where ε_r and η are, respectively, the relative permittivity and viscosity of the electrolyte solution and ε_0 is the permittivity of vacuum. This equation is valid when $\kappa\, a$ is sufficiently large ($\kappa\, a \gg 1$), where a is the hydrodynamic radius of the particle and κ is the Debye-Hückel parameter. The reciprocal of k ($1/\kappa$) which is called the Debye length corresponds to the thickness of the diffuse double layer

$$\frac{1}{\kappa} = \left(\frac{\varepsilon_r \varepsilon_0 kT}{\sum_{i=1}^{N} z_i e^2 n_i^{\infty}} \right)^{1/2} \tag{2}$$

where T is the absolute temperature, k is the Boltzmann's constant, z_i is the valence of ions, e is the elementary electric charge, and n_i^{∞} is the bulk concentration (number density).

Adsorption experiments

Dye concentration was determined to a UV–Vis spectrophotometer (Evolution 300, Thermo) using the maximum absorbance of AB113 dye ($\lambda_{max} = 581$ nm). The pH of AB113 solution was adjusted with HCl (0.1 and 0.01 mol L^{-1}) or NaOH (0.1 and 0.01 mol L^{-1}). All adsorption experiments were conducted in duplicate under 300 rpm stirring using a thermostatic bath.

Adsorption kinetics

To perform the adsorption kinetics, 50 mg of MC was added to 100 mL of AB113 (150 mg L^{-1}, at 298 K and pH = 7.0). Aliquots at different time intervals (0–300 min) were collected to determine the residue concentration of dye in the solution. Models used to simulate kinetic data are supplied in the Supplementary Information.

Adsorbent dosage

To investigate the effect of adsorbent dosage, different MC mass dosage (5 to 75 mg) was added to 100 mL of AB113 (150 mg L^{-1}, at 298 K and pH = 7.0). After 300 min, aliquots were collected and analyzed.

Effect of pH value and ionic strength for AB113 adsorption onto MC

The effect of the initial pH value on AB113 adsorption on MC was evaluated by adding 50 mg of MC to 100 mL of AB113 (150 mg L^{-1}, at 298 K) with different pH values (from 3 to 11).

To investigate the effect of ionic strength, 50 mg of MC was added to 100 mL of AB113 (150 mg L^{-1}, at 298 K and pH = 7.0) with different NaCl concentrations (from 0 to 0.5 mol L^{-1}).

Adsorption isotherms

The adsorption isotherms were performed at 288, 298, and 308 K by adding 50 mg of MC to 100 mL of AB113 at pH = 7.0 with concentrations ranging from 25 to 250 mg L^{-1}. After 300 min, aliquots were collected and analyzed.

The amount of dye adsorbed q_e (mg g^{-1}) was given according to Eq. 3:

$$q_e = \frac{(C_o - C_t) \times V}{m} \tag{3}$$

where C_0 (mg L^{-1}) is the initial adsorbate concentration, C_t (mg L^{-1}) is the concentration of adsorbate at time t (min), V (L) is the solution volume, m (g) is the mass of the adsorbent, and q_e (mg g^{-1}) is the adsorbed amount at time t (min). Models used to simulate the adsorption isotherms data are supplied in the Supplementary Information.

Thermodynamic study

Based on the adsorption isotherms, the thermodynamic parameters enthalpy (ΔH), entropy (ΔS), and Gibbs free energy (ΔG) were determined by the following equations:

$$\Delta G^{\circ} = -RT ln K_{ad} \tag{4}$$

$$ln k_{ad} = -\Delta H^{\circ}/RT + \Delta S^{\circ}/R \tag{5}$$

where k_{ad} is the Langmuir constant (L mg^{-1}) obtained in each adsorption isotherm multiplied by the density of water (10^6 mg L^{-1}) (Yu et al. 2015).

Regeneration and reuse of MC

After the first adsorption cycle using 75 mg of MC to 150 mL of AB113 (150 mg L^{-1}, at 298 K and pH 7.0), the spent adsorbent was separated and dispersed into 10 mL of $Fe(NO_3)0.6H_2O$ aqueous solution (0.00011 mol L^{-1}) and 0.00097 mol L^{-1} of H_2O_2 under sunlight. After 1 h of reaction, MC was separated, dried at 353 K, and then reused. The $Fe(NO_3)$ $6H_2O$ solution was reused in all recycles. To

compare the regeneration of MC by photo-Fenton proposed here, the reuse study of the adsorbent was also carried out without the regeneration process. In this case, the adsorbent was only separated and dried at 353 K.

Results and discussion

Characterization of mesoporous carbon

XRD patterns of Laponite/starch composite and MC are shown in Fig. 1a. For the Laponite/starch composite, the XRD pattern shows peaks with several orders of basal reflection (*00 l*), evidencing the presence of an ordered layered structure (Perotti et al. 2014; Pinto et al. 2016). The basal spacing of Laponite with starch was calculated with the Bragg equation, using the peak position (001). According to the result obtained, the basal spacing was 2.26 nm indicating the incorporation of multiple chains of amylose/amylopectin molecules between the Laponite layers. A similar arrangement was previously observed for other biopolymers intercalated in different clays, such as chitosan in montmorillonite (Tan et al. 2008; Li et al. 2019) and starch in Laponite (Perotti et al. 2014; Pinto et al. 2016).

The graphitization degree of the MC was determined by XRD and Raman spectroscopy. XRD pattern (Fig. 1a) shows one broad peak around at $2\theta = 24.3°$ assigned to the (002) plane of the turbostratic carbon structure (a disordered form of the graphitic structure) with the distance between graphene layers of 3.66 Å (Li et al. 2007; Song et al. 2015).

To evaluate the ordering level (crystallinity and defect/disorder) of MC, Raman spectroscopy analysis was performed (Fig. 1b). The Raman spectra show that the D band (ca. 1327 cm^{-1}) is more intense than the G band (ca. 1587 cm^{-1}), indicating the presence of disordered carbon in the MC, confirming indications from the XRD analysis. Besides, the intensity ratio of the D and G bands showed a 1.12 ratio, which indicates that this material has amorphous carbon and/or structural defects because materials with a low-intensity ratio ($I_D/I_G < 0.8$) such as carbon nanotube or graphite has a tiny amount of amorphous carbon or structural defects (Pimenta et al. 2007; Lucchese et al. 2010). Thus, the lower the ratio, the higher the graphitization. These results (XRD and Raman) reveal that the MC contains crystalline carbon of turbostratic structure with some amount of highly disordered amorphous carbon.

Figure 2 presents the N_2 physisorption isotherm and the BJH pore size distribution curve for MC. According to IUPAC classification, the MC isotherm is classified as type IV with a hysteresis of type H1, characteristic of mesoporous solids with uniform pore size. The MC specific area, pore volume, and average pore size were 1008 $m^2\ g^{-1}$, 1.67 $cm^3\ g^{-1}$, and 5 nm, respectively.

When the textural properties, like surface area and pore volume of MC, are compared with other mesoporous carbons reported in the scientific literature (Table S1), the MC generally presents higher porosity values. Materials such as ordered mesoporous carbon (MCS/C), which present higher or similar porosity to MC, are disadvantaged over MC because of the high costs of their precursors and complex methods of preparation (Teng et al. 2013). Furthermore, MC presents a carbon source of renewable origin.

The SEM images (Fig. 3) reveal that the presence of Laponite contributed to defining MC shape and texture. As discussed in the XRD analysis, the intercalation has been noted for the composite, which allows for predicting the occurrence of alternation in the overlap of layers of clay and the polymer. After the pyrolysis and acid washing, the overlapping of carbon layers was observed, with empty spaces referring to the removal of Laponite. Such information and

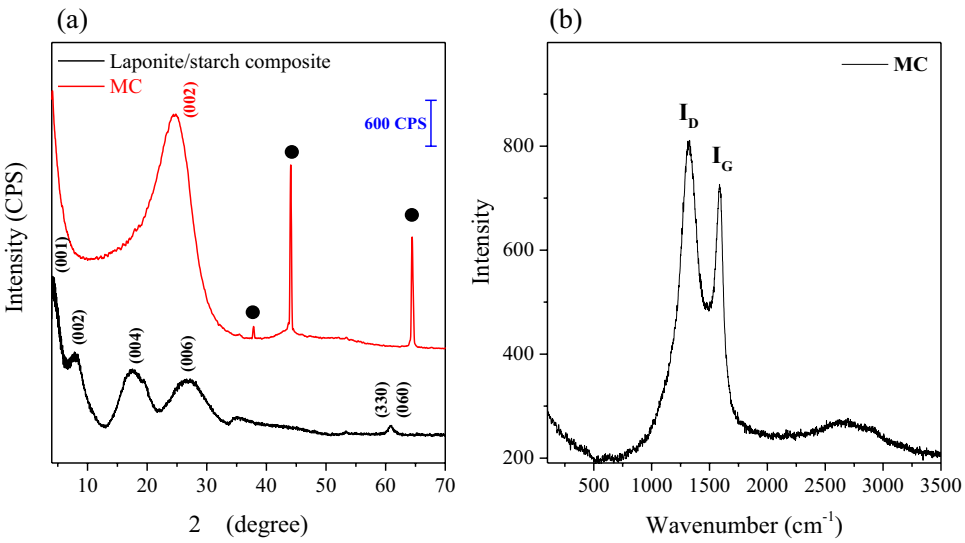

Fig. 1 **a** XRD patterns of Laponite/starch composite and MC (● Al from sample holder) and **b** Raman spectrum of MC

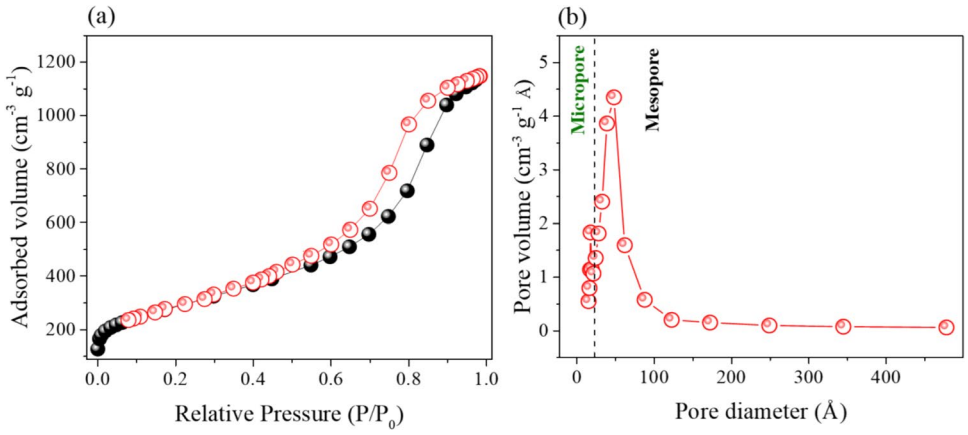

Fig. 2 **a** N_2 adsorption/desorption isotherm of MC; **b** pore size distribution of the materials from N_2 adsorption branch by the BJH method

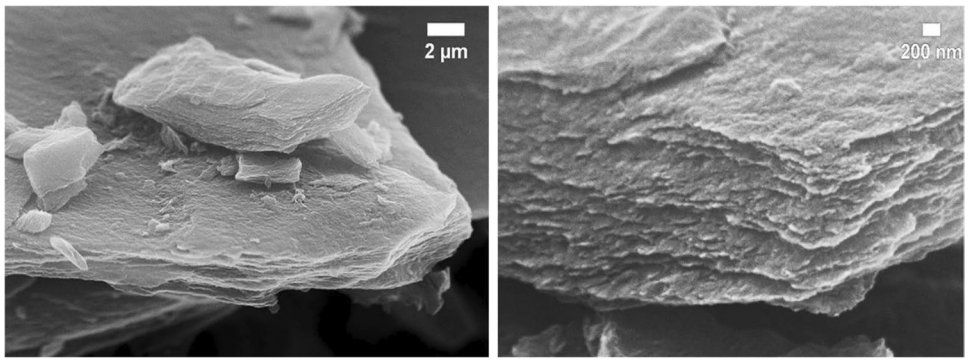

Fig. 3 SEM images at different magnifications (10,000 and 50,000 times) of MC

the SEM image demonstrate that the pores of this material are between the carbon layers.

AB113 adsorption

The effect of contact time on the AB113 adsorption (Fig. 4a) shows that the time required for adsorption to reach equilibrium was 1.5 h and that most of the adsorption took place during the first 30 min after the addition of MC. Based on the obtained results, 1.5 h was selected as the equilibrium time for the rest of the experiments.

The adsorption rate and the expression that describes the adsorption mechanism were determined using pseudo–first-order, pseudo–second-order, and intraparticle diffusion models (Table 1). According to the results, the experimental data was best fitted using the pseudo–second-order model, showing that the process is controlled by chemical adsorption.

The effect of ionic strength was evaluated by adding different concentrations of NaCl (Fig. 4b). As can be seen, an increase in ionic strength provides an increase in the AB113 adsorption. This effect promoted by NaCl addition can be explained by Fig. 4c, which shows the influence of pH on the ζ-potential values of MC particles at different ionic strengths. It is observed that the surface of MC has a negative charge at neutral pH. The ζ-potential values change from negative to positive at pH = 3.9, indicating the presence of an isoelectric point. The pH at which $\zeta = 0$ mV is called the isoelectric point (I.Z.P) (Hunter and Hunter 1981a). The I.Z.P of MC particles is not affected by the increase in ionic strength. The fact that I.Z.P is independent of the electrolyte concentration suggests that (I) the I.Z.P is, in this case, the same as the zero charge point (P.Z.C) and (II) NaCl is an indifferent electrolyte for MC particles (Hunter and Hunter 1981a). An important effect of the indifferent electrolyte is that it strongly influences the magnitude of the ζ-potential values. The electrolyte concentration increases cause an increase in the Debye-Hückel parameter, because of which the electrical potential falls off more rapidly at the surface (Hunter and Hunter 1981b). This effect is referred to as "compression of the diffuse double layer." Therefore, the addition of salt decreases the electrostatic repulsion of the negatively charged surface of MC particles and the anionic dye AB113. At the same time, the increase in the concentration of NaCl may also have promoted the dimerization of the dye, contributing to the increase in the adsorption capacity (Al-Degs et al. 2008).

The effect of pH on the AB113 removal (Fig. 4d) shows that the adsorption capacity decreases from 335.0 to 150 mg g^{-1} with the pH increases. This effect on the variation of the adsorption capacity can be explained by

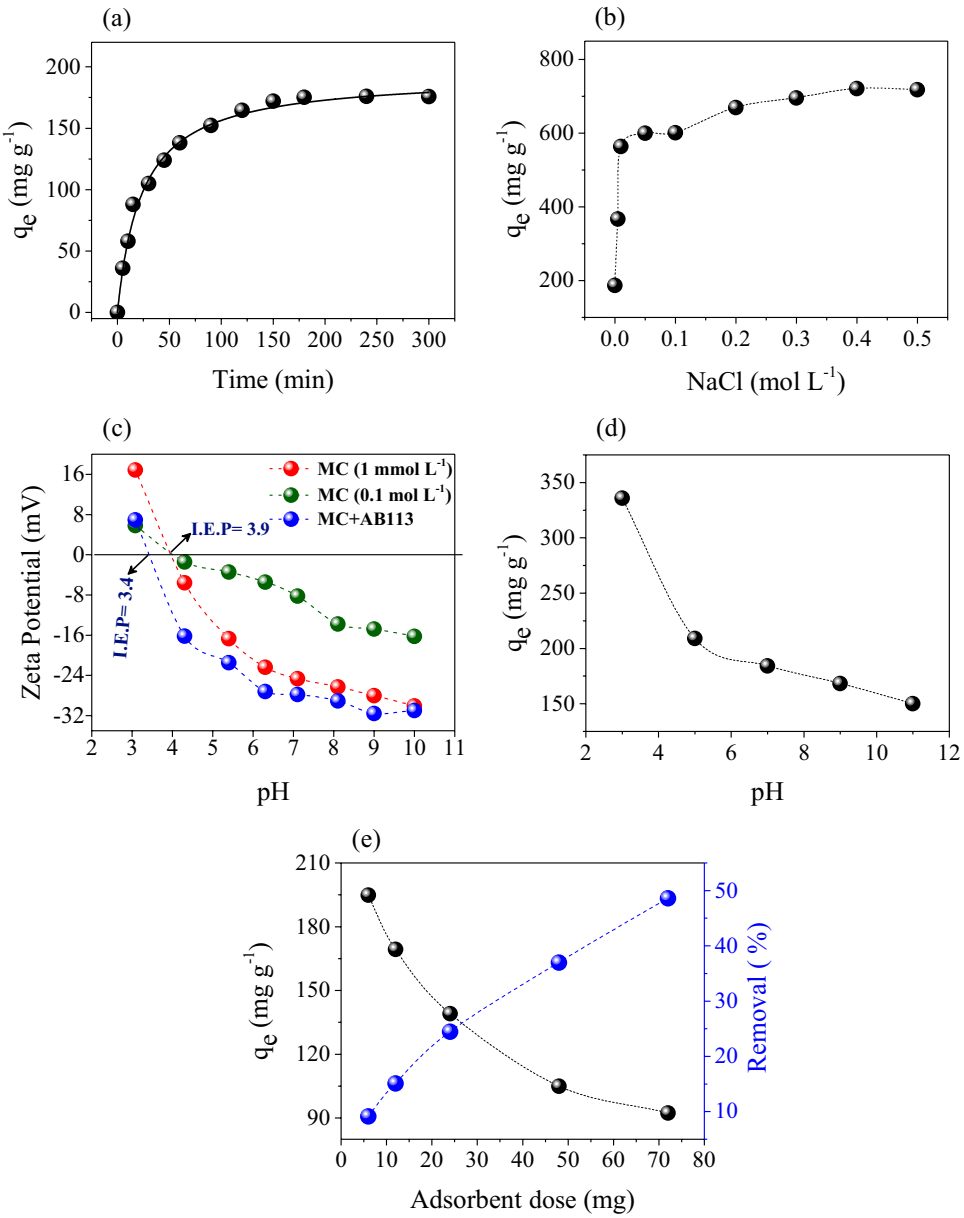

Fig. 4 **a** Effect of contact time (AB113 concentration = 150 mg L^{-1}, MC = 0.50 g L^{-1}, and T = 298 K), **b** effect of ionic strength (AB113 concentration = 150 mg L^{-1}, MC = 0.50 g L^{-1}, and T = 298 K), **c** zeta potential of MC particles as a function of pH at different NaCl concentrations, **d** effect of pH (AB113 concentration = 150 mg L^{-1}, MC = 0.50 g L^{-1}, and T = 298 K), and **e** effect of MC dosage for dye adsorption (AB113 concentration = 150 mg $L.^{-1}$ and T = 298 K)

Table 1 Kinetic parameters for the adsorption of AB113 on MC

Pseudo–first order			Pseudo–second order			Intraparticle diffusion		
k_1 (h^{-1})	q_e (mg/g)	R^2	k_2 (g/mg h) 10^{-3}	q_e (mg/g)	R^2	K_i (mg/g h)	C (mg/g)	R^2
27.5	143.9	0.60	21.9	193.7	0.988	6.00	82.11	0.577

the surface charge of MC, as the molecules of AB113 dye (pKa = 0.5) are in anionic form in the studied pH range (Mohammadzadeh et al. 2015). Thus the surface of MC at low pH values is positively charged (pH < pHI.Z.P) which favors the electrostatic attractions between the anionic dye and the surface of MC particles; already at pH values greater than 3.9 (pH > pHI.Z.P), the material is negatively charged.

After adsorption of dye AB113, the I.Z.P of MC particles changes from 3.9 to 3.3 (Fig. 4c). The change in I.Z.P is caused by ions or molecules that have a chemical or specific affinity for the surface, in addition to purely Coulomb interactions (Hunter and Hunter 1981a). Based on these results, it can be concluded that as well as to the π-type interactions that occur between carbon-based materials and organic molecules, electrostatic interactions also influence

the adsorption mechanism (Ma et al. 2012; Gupta and Khatri 2019).

Figure 5 shows the AB113 adsorption as a function of MC mass (5–72 mg). As can be seen, the increase of the amount of MC increased the removal percent (10% to 50%) and decreased the amount of adsorbed dye (q_e) (200 to 90 mg g^{-1}). This behavior is consistent with the increase in the number of adsorption sites; thus the increase in removal percent can be explained by the amount increase of adsorption sites with the increase in MC mass, while that the q_e decreases due to the unsaturation of available adsorption sites, leading to a lower amount of dye adsorbed per unit weight of MC (Eq. 3). Similar trends are reported (Silva et al. 2018; Arabkhani and Asfaram 2020).

Adsorption isotherms

To provide information about the surface properties of MC, adsorption mechanisms, the affinity, and estimate of the adsorption capacity were performed by the equilibrium adsorption isotherm. In this study, the experimental data were fitted by the nonlinear Langmuir and Freundlich equation. The adsorption behavior of AB113 onto MC at 288 K, 298 K, and 308 K is shown in Fig. 5a.

As shown in Fig. 5a and Table 2, the Langmuir model yielded the best fit, thus indicating the existence of homogeneity of the surface of MC and that adsorption of each dye molecule has equal adsorption activation energy. The maximum adsorption capacity (q_{max}) and Langmuir constant (K_L) calculated based on adsorption isotherm are listed in Table 2. These results showed which AB113 adsorption increase with an increase in temperature, indicating that the affinity between the adsorbent and adsorbate grows (Chowdhury et al. 2011; Wu et al. 2014).

One evidence that explained the increase of adsorption capacity with the temperature increase is based on the electrostatic interactions between the surface of MC and the AB113. Figure 5b shows the behavior of the ζ-potential and the thickness of the diffuse double layer as a function of temperature. The MC particles present negative values of ζ-potential in the temperature range from 288 to 308 K. The ζ-potential ranges from − 28 mV at low temperatures to − 15 mV at higher temperatures. This behavior is attributed to the variation in the thickness of the double layer. The increase in temperature compresses the double layer formed around the particles of the MC, reducing the magnitude of the ζ-potential values, promoting a greater interaction between AB113 and MC, which end up favoring increased adsorption with an increase in temperature.

The effect of temperature for AB113 adsorption onto MC showed that a higher quantity of the dye is adsorbed with an increase of temperature, indicating an endothermic process. The plot of $ln\ K_{ad}$ versus $1/T$ shown in the Supplementary Information (Fig. S1) follows a straight line, and the slope and intercept coefficient values allow obtaining the values of ΔH° and ΔS°, respectively. The thermodynamic properties evaluated from the Van't Hoff plot are reported in Table 3.

The negative values of ΔG° confirm that the adsorption of AB113 onto MC was spontaneous and thermodynamically favorable and that temperature increase favors the

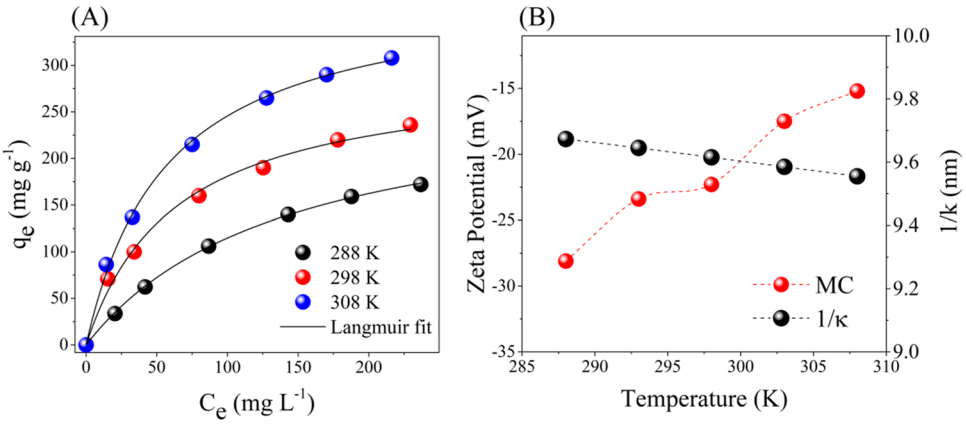

Fig. 5 **a** Equilibrium adsorption isotherms of AB113 onto MC, at 288, 298, and 308 K (AB113 concentration = 50–250 mg L^{-1}, $MC = 0.50$ g $L.^{-1}$). **b** Effect of the temperature on the zeta potential and in the thickness of the diffuse double-layer ($\frac{1}{\kappa}$) of MC particles

Table 2 Isotherm model parameters for the adsorption of AB113 onto MC

Temperature	Langmuir			Freundlich		
	q_{max} (mg/g)	K_L (L m/g)	R^2	K_F	N	R^2
288 K	277	0.00707	0.998	31.01	2.30	0.989
298 K	295	0.0158	0.997	22.49	2.28	0.987
308 K	360	0.0201	0.999	7.20	1.70	0.988

Table 3 Thermodynamic parameters at various temperatures

Temperature	Thermodynamic parameters		
	ΔG (kJ mol^{-1})	ΔH (kJ mol^{-1})	ΔS (kJ K^{-1} mol^{-1})
288 K	−21.23	38.78	0.209
298 K	−23.96		
308 K	−25.38		

adsorption. The positive value of ΔH° is related to the endothermic nature of the process, while the positive value of ΔS° suggests an increase in the disorder at the solid-solution interface.

Adsorption mechanism

The results obtained in this work indicate that the surface charge of the adsorbent can be modified by the conditions of the aqueous medium (temperature and ionic strength) and that the change of this charge also influences the adsorption capacity. Furthermore, it should be stressed, except for the study of the pH effect, in which the MC is positively charged at pH = 3, the other studies showed that both MC and AB113 (pKa = 0.5) were negatively charged, which theoretically did not favor adsorption. Therefore, the contribution of other mechanisms, such as the π-π electron acceptor interactions between MC and AB113 and the interaction via the mesopore filling mechanism, may be the main factors for explaining the adsorption of AB113, even under unfavorable load conditions (Ma et al. 2012; Yang et al. 2015; Asakawa et al. 2020; Ansari et al. 2022). The AB113 has single and double bonds between the C and contains π electrons; these π electrons can easily interact with the π electrons on the MC surface through π-π electron coupling (Ma et al. 2012; Cazetta et al. 2016). Furthermore, the dimensions of the AB113 molecule (2.3 nm × 1.0 nm × 0.48 nm, estimated by the Jmol software) are compatible with the average pore size of the MC (~ 5 nm), thus allowing wide accessibility of AB113 in the mesoporous of the MC.

Regeneration and reuse of MC

Regeneration and reuse of adsorbents are crucial for industrial applications due to the reduction of costs (Charumathi and Das 2012). MC regeneration by oxidation of the dye adsorbed with radicals (OH•) generated by the photo-Fenton reaction (Nogueira et al. 2005; Azha et al. 2019) is shown in Fig. 6.

The results obtained show that the maximum adsorption capacity after the regeneration process was 90%, 80%, and 54% concerning the "fresh" adsorbent, while the untreated MC has its adsorption capacity considerably reduced to 39%, 25%, and 10%, probably because of the saturation of the

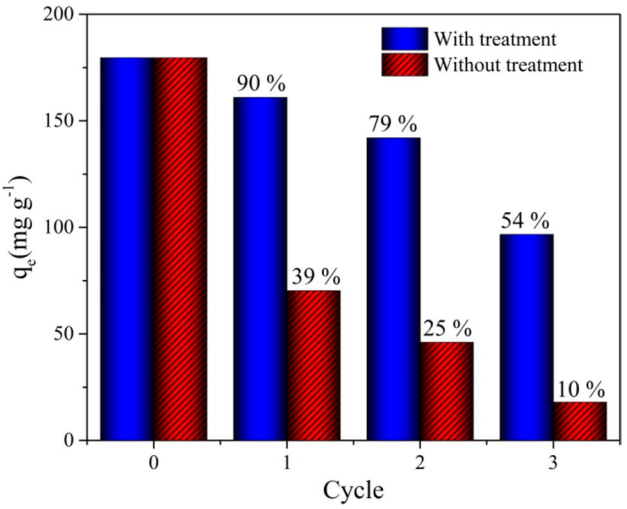

Fig. 6 Recycling of MC after adsorption (AB113 concentration = 150 mg L^{-1}, MC = 0.50 g L.$^{-1}$, and T = 298 K)

adsorption sites. These results show that the regeneration process by the photo-Fenton reaction is fast and low cost, due to the small amount of peroxide used and the facility to reuse the Fe^{3+} solution. In addition to the homogeneous photo-Fenton reaction used in this work to oxidize the pre-concentrated dye on the surface of the adsorbent, other promising techniques able to generate radicals such as OH• could be used in future studies to establish another way to the regeneration of the adsorbent. Among the methodologies, heterogeneous Fenton or photo-Fenton (Gonçalves et al. 2019, 2020) can be performed on carbon materials impregnated with oxides (e.g., iron, copper, or manganese). Another possible methodology is the sono-catalysis treatment (Amaniampong et al. 2017, 2018, 2019); this treatment was given highlighted as a very effective methodology in the degradation of organic compounds being able to continuously generate OH• radicals without using H_2O_2.

Conclusion

The results of AB113 adsorption onto MC showed that the adsorption kinetics and adsorption isotherm fit the pseudo–second-order kinetic model and Langmuir model very well, indicating that the adsorption rate is controlled by the chemisorption and that each dye molecule has equal adsorption activation energy onto the surface of MC. It is also shown that AB113 adsorption onto MC (295 mg g^{-1} at pH = 7.0 and 298 K) is significantly higher compared to the different types of carbon-based materials reported in the literature (Table S2). The higher adsorption capacity of MC is probably due to its large surface area and pore volume. The AB113 adsorption capacity increases with the increase

of ionic strength and temperature. Zeta potential values indicated that the change of adsorption capacity of AB113 onto MC with the variation of ionic strength and temperature is due to the compression of the diffuse double layer of the surface of MC, promoting the decrease of electrostatic repulsion between MC and AB113. Thermodynamic results demonstrate that the adsorption process was spontaneous and endothermic. Moreover, for the first time, this work demonstrates that the temperature and the ionic strength of the aqueous medium are also able to change the surface charge of carbon-based adsorbents and surely influence the adsorption capacity. Finally, the regeneration of the adsorbent by the photo-Fenton reaction regenerated the adsorption capacity of the absorbent without generating secondary pollution to the environment.

Supplementary Information The online version contains supplementary material available at https://doi.org/10.1007/s11356-022-21193-y.

Acknowledgements The authors are grateful to CAPES, CNPq, and FAPEMIG for financial support and CAPQ-UFLA for the analytical results.

Author contribution RGLG is the main author contributing in all steps. PAL performed the adsorption experiments. DJP performed the zeta potential analysis. LCAO, FGP, JLN, and JT worked on the Results and discussion. All the authors read and commented on the manuscript.

Availability of data and materials All data generated or analyzed during this study are included in this published article.

Declarations

Ethics approval The authors declare that they submit original work as a whole, not published elsewhere, that the results are not falsified, and that proper acknowledgements to other works have been given.

Competing interests The authors declare no competing interests.

References

Agnihotri SM, Ohshima H, Terada H et al (2009) Electrophoretic mobility of colloidal gold particles in electrolyte solutions. Langmuir. https://doi.org/10.1021/la803671t

Al-Degs YS, El-Barghouthi MI, El-Sheikh AH, Walker GM (2008) Effect of solution pH, ionic strength, and temperature on adsorption behavior of reactive dyes on activated carbon. Dye Pigment 77:16–23. https://doi.org/10.1016/j.dyepig.2007.03.001

Amaniampong PN, Karam A, Trinh QT et al (2017) Selective and Catalyst-free Oxidation of D-Glucose to D-Glucuronic acid induced by High-Frequency Ultrasound. Sci Reports 71(7):1–8. https://doi.org/10.1038/srep40650

Amaniampong PN, Trinh QT, De Oliveira Vigier K et al (2019) Synergistic effect of high-frequency ultrasound with cupric oxide catalyst resulting in a selectivity switch in glucose oxidation under argon. J Am Chem Soc 141:14772–14779. https://doi.org/10.1021/jacs.9b06824

Amaniampong PN, Trinh QT, Varghese JJ et al (2018) Unraveling the mechanism of the oxidation of glycerol to dicarboxylic acids over a sonochemically synthesized copper oxide catalyst. Green Chem 20:2730–2741. https://doi.org/10.1039/C8GC00961A

Ansari KB, Gaikar VG, Trinh QT et al (2022) Carbon dioxide capture over amine functionalized styrene divinylbenzene copolymer: An experimental batch and continuous studies. J Environ Chem Eng 10:106910. https://doi.org/10.1016/j.jece.2021.106910

Arabkhani P, Asfaram A (2020) Development of a novel three-dimensional magnetic polymer aerogel as an efficient adsorbent for malachite green removal. J Hazard Mater 384:121394. https://doi.org/10.1016/J.JHAZMAT.2019.121394

Asakawa H, Matsui S, Trinh QT et al (2020) Chiral Monolayers with Achiral Tetrapod Molecules on Highly Oriented Pyrolytic Graphite. J Phys Chem C 124:7760–7767. https://doi.org/10.1021/acs.jpcc.9b11246

Azam K, Raza R, Shezad N et al (2020) Development of recoverable magnetic mesoporous carbon adsorbent for removal of methyl blue and methyl orange from wastewater. J Environ Chem Eng 8:104220. https://doi.org/10.1016/j.jece.2020.104220

Azha SF, Sellaoui L, Engku Yunus EH et al (2019) Iron-modified composite adsorbent coating for azo dye removal and its regeneration by photo-Fenton process: synthesis, characterization and adsorption mechanism interpretation. Chem Eng J 361:31–40. https://doi.org/10.1016/J.CEJ.2018.12.050

Borrely SI, Rosa JM, Boiani NF, Garcia VS, Sousa AL (2018) Emerging pollutants, related toxicity, and water quality decreasing: tannery, textile, and pharmaceuticals load pollutants. Biol Eng Med 3:1–6. https://doi.org/10.15761/bem.1000157

Cao M, Li Y, Yin H, Shen S (2019) Functionalized graphene nanosheets as absorbent for copper(II) removal from water. Ecotoxicol Environ Saf 173:28–36. https://doi.org/10.1016/J.ECOENV.2019.02.011

Cazetta AL, Pezoti O, Bedin KC et al (2016) Magnetic activated carbon derived from biomass waste by concurrent synthesis: Efficient adsorbent for toxic dyes. ACS Sustain Chem Eng 4:1058–1068. https://doi.org/10.1021/acssuschemeng.5b01141

Charumathi D, Das N (2012) Packed bed column studies for the removal of synthetic dyes from textile wastewater using immobilised dead C. tropicalis. Desalination 285:22–30. https://doi.org/10.1016/j.desal.2011.09.023

Chen C, Gunawan P, Xu R (2011) Self-assembled Fe3O4-layered double hydroxide colloidal nanohybrids with excellent performance for treatment of organic dyes in water. J Mater Chem 21:1218. https://doi.org/10.1039/c0jm01696a

Chiang CH, Chen J, Lin JH (2020) Preparation of pore-size tunable activated carbon derived from waste coffee grounds for high adsorption capacities of organic dyes. J Environ Chem Eng 8:103929. https://doi.org/10.1016/j.jece.2020.103929

Chowdhury S, Mishra R, Saha P, Kushwaha P (2011) Adsorption thermodynamics, kinetics and isosteric heat of adsorption of malachite green onto chemically modified rice husk. Desalination 265:159–168. https://doi.org/10.1016/j.desal.2010.07.047

da Silva JS, da Rosa MP, Beck PH et al (2018) Preparation of an alternative adsorbent from Acacia mearnsii wastes through acetosolv method and its application for dye removal. J Clean Prod 180:386–394. https://doi.org/10.1016/J.JCLEPRO.2018.01.201

dos Santos A, Viante MF, Pochapski DJ et al (2018) Enhanced removal of p-nitrophenol from aqueous media by montmorillonite clay modified with a cationic surfactant. J Hazard Mater 355:136–144. https://doi.org/10.1016/J.JHAZMAT.2018.02.041

Du F, Sun L, Huang Z et al (2020) Electrospun reduced graphene oxide/TiO2/poly(acrylonitrile-co-maleic acid) composite nanofibers for efficient adsorption and photocatalytic removal of malachite green and leucomalachite green. Chemosphere

239:124764. https://doi.org/10.1016/J.CHEMOSPHERE.2019.124764
Fahel J, Kim S, Durand P et al (2016) Enhanced catalytic oxidation ability of ternary layered double hydroxides for organic pollutants degradation. Dalton Trans 45:8224–8235. https://doi.org/10.1039/c6dt00441e
Gonçalves RGL, Lopes PA, Resende JA et al (2019) Performance of magnetite/layered double hydroxide composite for dye removal via adsorption, Fenton and photo-Fenton processes. Appl Clay Sci 179:105152. https://doi.org/10.1016/J.CLAY.2019.105152
Gonçalves RGL, Mendes HM, Bastos SL et al (2020) Fenton-like degradation of methylene blue using Mg/Fe and MnMg/Fe layered double hydroxides as reusable catalysts. Appl Clay Sci 187:105477. https://doi.org/10.1016/J.CLAY.2020.105477
Gupta K, Khatri OP (2019) Fast and efficient adsorptive removal of organic dyes and active pharmaceutical ingredient by microporous carbon: effect of molecular size and charge. Chem Eng J 378:122218. https://doi.org/10.1016/J.CEJ.2019.122218
Gupta VK, Gupta B, Rastogi A et al (2011) A comparative investigation on adsorption performances of mesoporous activated carbon prepared from waste rubber tire and activated carbon for a hazardous azo dye—Acid Blue 113. J Hazard Mater 186:891–901. https://doi.org/10.1016/J.JHAZMAT.2010.11.091
Hamza W, Dammak N, Hadjltaief HB et al (2018) Sono-assisted adsorption of Cristal Violet dye onto Tunisian Smectite Clay: characterization, kinetics and adsorption isotherms. Ecotoxicol Environ Saf 163:365–371. https://doi.org/10.1016/J.ECOENV.2018.07.021
Hao Y, Wang Z, Wang Z, He Y (2019) Preparation of hierarchically porous carbon from cellulose as highly efficient adsorbent for the removal of organic dyes from aqueous solutions. Ecotoxicol Environ Saf 168:298–303. https://doi.org/10.1016/J.ECOENV.2018.10.076
Hu X, Jia L, Cheng J, Sun Z (2019) Magnetic ordered mesoporous carbon materials for adsorption of minocycline from aqueous solution: preparation, characterization and adsorption mechanism. J Hazard Mater 362:1–8. https://doi.org/10.1016/J.JHAZMAT.2018.09.003
Hunter RJ, Hunter RJ (1981a) Applications of the zeta potential. Zeta Potential Colloid Sci:219–257. https://doi.org/10.1016/B978-0-12-361961-7.50010-9
Hunter RJ, Hunter RJ (1981b) The calculation of zeta potential. Zeta Potential Colloid Sci:59–124.https://doi.org/10.1016/B978-0-12-361961-7.50007-9
Ip AWM, Barford JP, McKay G (2009) Reactive black dye adsorption/desorption onto different adsorbents: effect of salt, surface chemistry, pore size and surface area. J Colloid Interface Sci 337:32–38. https://doi.org/10.1016/j.jcis.2009.05.015
Lellis B, Fávaro-Polonio CZ, Pamphile JA, Polonio JC (2019) Effects of textile dyes on health and the environment and bioremediation potential of living organisms. Biotechnol Res Innov 3:275–290. https://doi.org/10.1016/J.BIORI.2019.09.001
Li J, Cai J, Zhong L et al (2019) Adsorption of reactive red 136 onto chitosan/montmorillonite intercalated composite from aqueous solution. Appl Clay Sci 167:9–22. https://doi.org/10.1016/J.CLAY.2018.10.003
Li ZQ, Lu CJ, Xia ZP et al (2007) X-ray diffraction patterns of graphite and turbostratic carbon. Carbon N Y 45:1686–1695. https://doi.org/10.1016/J.CARBON.2007.03.038
Liu Q, Li Y, Chen H et al (2020) Superior adsorption capacity of functionalised straw adsorbent for dyes and heavy-metal ions. J Hazard Mater 382:121040. https://doi.org/10.1016/J.JHAZMAT.2019.121040
Lucchese MM, Stavale F, Ferreira EHM et al (2010) Quantifying ion-induced defects and Raman relaxation length in graphene. Carbon N Y 48:1592–1597. https://doi.org/10.1016/J.CARBON.2009.12.057
Luo Y, Guo W, Ngo HH et al (2014) A review on the occurrence of micropollutants in the aquatic environment and their fate and removal during wastewater treatment. Sci Total Environ 473–474:619–641. https://doi.org/10.1016/j.scitotenv.2013.12.065
Ma J, Yu F, Zhou L et al (2012) Enhanced adsorptive removal of methyl orange and methylene blue from aqueous solution by alkali-activated multiwalled carbon nanotubes. ACS Appl Mater Interfaces 4:5749–5760. https://doi.org/10.1021/am301053m
Marrakchi F, Hameed BH, Bouaziz M (2020) Mesoporous and high-surface-area activated carbon from defatted olive cake by-products of olive mills for the adsorption kinetics and isotherm of methylene blue and acid blue 29. J Environ Chem Eng 8:104199. https://doi.org/10.1016/j.jece.2020.104199
Mohammadzadeh S, Olya ME, Arabi AM et al (2015) Synthesis, characterization and application of ZnO-Ag as a nanophotocatalyst for organic compounds degradation, mechanism and economic study. J Environ Sci 35:194–207. https://doi.org/10.1016/J.JES.2015.03.030
Nogueira RFP, Silva MRA, Trovó AG (2005) Influence of the iron source on the solar photo-Fenton degradation of different classes of organic compounds. Sol Energy 79:384–392. https://doi.org/10.1016/j.solener.2005.02.019
Parker HL, Hunt AJ, Budarin VL et al (2012) The importance of being porous: polysaccharide-derived mesoporous materials for use in dye adsorption. RSC Adv 2:8992–8997. https://doi.org/10.1039/c2ra21367b
Perotti GF, Tronto J, Bizeto MA et al (2014) Biopolymer-clay nanocomposites: cassava starch and synthetic clay cast films. J Braz Chem Soc 25:320–330. https://doi.org/10.5935/0103-5053.20130300
Pimenta MA, Dresselhaus G, Dresselhaus MS et al (2007) Studying disorder in graphite-based systems by Raman spectroscopy. Phys Chem Chem Phys 9:1276–1290. https://doi.org/10.1039/B613962K
Pinto M de CE, Lima RG, dos Santos RMM et al (2016) Mesoporous carbon derived from a biopolymer and a clay: preparation, characterization and application for an organochlorine pesticide adsorption. Microporous Mesoporous Mater 225:342–354. https://doi.org/10.1016/j.micromeso.2016.01.012
Pinto MCE, Santos RMM, Gonçalves RGL et al (2018) Adsorption of dicamba herbicide onto a carbon replica obtained from a layered double hydroxide. Dalton Trans 47:3119–3127. https://doi.org/10.1039/c7dt03720a
Qiang Z, Gurkan B, Ma J et al (2016) Roll-to-roll fabrication of high surface area mesoporous carbon with process-tunable pore texture for optimization of adsorption capacity of bulky organic dyes. Microporous Mesoporous Mater 227:57–64. https://doi.org/10.1016/J.MICROMESO.2016.02.015
Rajumon R, Anand JC, Ealias AM et al (2019) Adsorption of textile dyes with ultrasonic assistance using green reduced graphene oxide: an in-depth investigation on sonochemical factors. J Environ Chem Eng 7:103479. https://doi.org/10.1016/j.jece.2019.103479
Samarghandi MR, Tari K, Shabanloo A et al (2020) Synergistic degradation of acid blue 113 dye in a thermally activated persulfate (TAP)/ZnO-GAC oxidation system: Degradation pathway and application for real textile wastewater. Sep Purif Technol 247:116931. https://doi.org/10.1016/J.SEPPUR.2020.116931
Singh SC, ElKabbash M, Li Z et al (2020) Solar-trackable superwicking black metal panel for photothermal water sanitation. Nat Sustain. https://doi.org/10.1038/s41893-020-0566-x
Song S, Ma F, Wu G et al (2015) Facile self-templating large scale preparation of biomass-derived 3D hierarchical porous carbon

for advanced supercapacitors. J Mater Chem A 3:18154–18162. https://doi.org/10.1039/C5TA04721H

Taffarel SR, Rubio J (2010) Adsorption of sodium dodecyl benzene sulfonate from aqueous solution using a modified natural zeolite with CTAB. Miner Eng 23:771–779. https://doi.org/10.1016/j.mineng.2010.05.018

Tan W, Zhang Y, Szeto Y, Liao L (2008) A novel method to prepare chitosan/montmorillonite nanocomposites in the presence of hydroxy-aluminum oligomeric cations. Compos Sci Technol 68:2917–2921. https://doi.org/10.1016/j.compscitech.2007.10.007

Teng W, Wu Z, Fan J et al (2013) Ordered mesoporous carbons and their corresponding column for highly efficient removal of microcystin-LR. Energy Environ Sci 6:2765–2776. https://doi.org/10.1039/C3EE41775A

Tian C, Feng C, Wei M, Wu Y (2018) Enhanced adsorption of anionic toxic contaminant Congo Red by activated carbon with electropositive amine modification. Chemosphere 208:476–483. https://doi.org/10.1016/J.CHEMOSPHERE.2018.06.005

Tokudome Y, Fukui M, Tarutani N et al (2016) High-density protein loading on hierarchically porous layered double hydroxide composites with a rational mesostructure. Langmuir 32:8826–8833. https://doi.org/10.1021/ACS.LANGMUIR.6B01925

Vecitis CD, Gao G, Liu H (2011) Electrochemical carbon nanotube filter for adsorption, desorption, and oxidation of aqueous dyes and anions. J Phys Chem C 115:3621–3629. https://doi.org/10.1021/jp111844j

Vikrant K, Giri BS, Raza N et al (2018) Recent advancements in bioremediation of dye: Current status and challenges. Bioresour Technol 253:355–367. https://doi.org/10.1016/J.BIORTECH.2018.01.029

Wu Z, Zhong H, Yuan X et al (2014) Adsorptive removal of methylene blue by rhamnolipid-functionalized graphene oxide from wastewater. Water Res 67:330–344. https://doi.org/10.1016/j.watres.2014.09.026

Xu J, Cao Z, Zhang Y et al (2018) A review of functionalized carbon nanotubes and graphene for heavy metal adsorption from water: preparation, application, and mechanism. Chemosphere 195:351–364. https://doi.org/10.1016/J.CHEMOSPHERE.2017.12.061

Xu S, Niu X, Hou Z et al (2020) A multifunctional gelatine–quaternary ammonium copolymer: an efficient material for reducing dye emission in leather tanning process by superior anionic dye adsorption. J Hazard Mater 383:121142. https://doi.org/10.1016/J.JHAZMAT.2019.121142

Yagub MT, Sen TK, Afroze S, Ang HM (2014) Dye and its removal from aqueous solution by adsorption: A review. Adv Colloid Interface Sci 209:172–184. https://doi.org/10.1016/J.CIS.2014.04.002

Yang G, Tang L, Zeng G et al (2015) Simultaneous removal of lead and phenol contamination from water by nitrogen-functionalized magnetic ordered mesoporous carbon. Chem Eng J 259:854–864. https://doi.org/10.1016/j.cej.2014.08.081

Yu Q, Zheng Y, Wang Y et al (2015) Highly selective adsorption of phosphate by pyromellitic acid intercalated ZnAl-LDHs: assembling hydrogen bond acceptor sites. Chem Eng J 260:809–817. https://doi.org/10.1016/j.cej.2014.09.059

Zhang P, Liu Y, Li Z et al (2018) Sorption and desorption characteristics of anionic surfactants to soil sediments. Chemosphere 211:1183–1192. https://doi.org/10.1016/J.CHEMOSPHERE.2018.08.051